

Evolution of elliptic and triangular flow as a function of $\sqrt{s_{NN}}$ in a hybrid model

Jussi Auvinen*

*Frankfurt Institute for Advanced Studies (FIAS),
Ruth-Moufang-Strasse 1, D-60438 Frankfurt am Main, Germany*

Hannah Petersen†

*Frankfurt Institute for Advanced Studies (FIAS),
Ruth-Moufang-Strasse 1, D-60438 Frankfurt am Main, Germany and
Institut für Theoretische Physik, Goethe Universität,
Max-von-Laue-Strasse 1, 60438 Frankfurt am Main, Germany*

Abstract

We study the collision energy dependence of elliptic flow v_2 and triangular flow v_3 in Au+Au collisions within the energy range $\sqrt{s_{NN}} = 5 - 200$ GeV, utilizing a transport + hydrodynamics hybrid model. The transport part is described by the Ultrarelativistic Quantum Molecular Dynamics (UrQMD) approach, combined with an intermediate (3+1)-dimensional ideal hydrodynamical evolution phase using a chiral model equation of state. We find the decrease of v_2 produced by hydrodynamics at lower collision energies partially compensated by the transport dynamics. This does not apply to v_3 , which falls to 0 in midcentral collisions at $\sqrt{s_{NN}} = 5$ GeV. We conclude that the triangular flow provides the clearer signal for the formation of low-viscous fluid in heavy ion collisions.

PACS numbers: 24.10.Lx, 24.10.Nz, 25.75.Ld

*Electronic address: auvinen@fias.uni-frankfurt.de

†Electronic address: petersen@fias.uni-frankfurt.de

I. INTRODUCTION

Several lattice calculations [1–3] have predicted the existence of a critical point in the QCD phase diagram, which marks the boundary of cross-over and first-order phase transition between the hadronic and QCD matter in the plane of baryochemical potential μ_B and temperature T . However, only the cross-over phase transition was seen in the continuum extrapolated results [4, 5]. In 2010, a beam energy scan program was launched at the Relativistic Heavy Ion Collider (RHIC) to study the features of the phase diagram and to investigate if any signals of a critical point can be found within the available range of μ_B .

By running experiments at different beam energies, collisions with varying peak temperatures and values of μ_B are produced that span a large region in the phase diagram of strongly interacting matter. So far, the scanned energy range reaches from $\sqrt{s_{NN}} = 200$ GeV down to 7.7 GeV, extending the baryochemical range from $\mu_B \sim 0$ up to ~ 400 MeV. Additional fixed target collisions down to ~ 3 GeV have been planned, which increase the μ_B -range even further [6]. This region of the phase diagram will also be the target for more detailed studies with much higher luminosities at the Facility for Antiproton and Ion Research (FAIR), which is currently under construction.

One of the key observables considered as the evidence of the formation of the strongly interacting matter, “quark-gluon plasma” (QGP) at RHIC and the Large Hadron Collider (LHC) is the elliptic flow, typically characterized by coefficient v_2 of the Fourier expansion of the azimuthal angle distribution of the final state particles. One would expect v_2 to decrease at lower beam energies, as the duration of the QGP phase gets smaller. However, the inclusive charged hadron v_2 has demonstrated surprisingly weak dependence on the collision energy between 7.7 and 39 GeV [7]. On the other hand, the preliminary results for the next Fourier coefficient v_3 , known as triangular flow, display a clearer change in magnitude for this observable between $\sqrt{s_{NN}} = 27 - 200$ GeV [8]. The weak energy dependence of the elliptic flow thus requires an explanation.

The beam energy dependence of the collective flow has been recently studied with several different models [9–14]. The method chosen for the present study is a hybrid approach, where a transport model – a microscopic description of the system – is utilized for the non-equilibrium phases at the beginning and in the end of a heavy-ion collision event, while a macroscopic hydrodynamical description is used to model the hot and dense intermediate

stage incorporating the phase transition between the QGP and hadronic matter. Such a hybrid model provides a consistent framework for investigating both high-energy heavy ion collisions with negligible net-baryon density and a large hydrodynamically evolving medium, and the collisions at smaller energies with finite net-baryon density, where no such medium is formed. Thus, this approach is optimal for studying the beam energy dependence of the elliptic and triangular flow.

The next Section provides a brief account of the main features of the applied hybrid model. The simulation results are presented in Section III. After comparing the transverse mass spectra of various particles against the experimental data in subsection III A, we study the elliptic and triangular flow in subsections III B and III C, respectively, concluding with an investigation of the dependence of flow coefficients on the initial collision geometry in III D. We then summarize our findings in Section IV.

II. HYBRID MODEL

This study was performed using a Boltzmann + hydrodynamics hybrid model described in [15]. In this framework, both the initial state before equilibrium and the final state with hadronic rescatterings and decays is calculated within the Ultrarelativistic Quantum Molecular Dynamics (UrQMD) string / hadronic cascade [16, 17].

The intermediate hydrodynamical evolution starts, when the two colliding nuclei have passed through each other:

$$t_{\text{start}} = \max\left\{\frac{2R}{\sqrt{\gamma_{CM}^2 - 1}}, 0.5 \text{ fm}\right\}, \quad (1)$$

where R represents the nuclear radius and $\gamma_{CM} = \frac{1}{\sqrt{1-v_{CM}^2}}$ is the Lorentz factor in the center-of-mass frame of the colliding nuclei. A minimum starting time of 0.5 fm is chosen based on the hybrid model results at the collision energy $\sqrt{s_{NN}} = 200$ GeV [18]. At this time, the energy-, momentum- and baryon number densities of the particles are mapped onto the hydro grid. The particles are represented by 3D Gaussian distributions that are Lorentz-contracted in the beam direction. The width parameter of these Gaussians is chosen to have the value $\sigma = 1.0$ fm to preserve the event-by-event initial state fluctuations. The spectator particles, which do not participate on the hydrodynamical evolution, are propagated separately in the cascade.

The evolution of the system in the intermediate phase is based on (3+1)-D ideal hydrodynamics, solving the evolution equations using the SHASTA algorithm [19, 20]. The equation of state (EoS) is based on a hadronic chiral parity doublet model including quark degrees of freedom and the thermal contribution of the Polyakov loop [21, 22]. This EoS qualitatively agrees with the lattice QCD data at $\mu_B = 0$ and, most importantly, is also applicable at finite baryon densities. After the last step of the hydrodynamical evolution, the active equation of state is changed from the deconfinement EoS to the hadron gas EoS, to ensure that the active degrees of freedom on both sides of the transition hypersurface are exactly equivalent [22].

The transition from hydro to transport, also known as “particlization”, is done when the energy density ϵ is smaller than the critical value $2\epsilon_0$, where $\epsilon_0 = 146 \text{ MeV}/\text{fm}^3$ represents the nuclear ground state energy density. This corresponds roughly to a switching temperature $T \approx 154 \text{ MeV}$ at $\sqrt{s_{NN}} = 200 \text{ GeV}$ Au+Au collisions [23]. While the switching criterion with respect to the energy density is kept constant over all collision energies, it will correspond to different combinations of temperature and baryochemical potential at different values of $\sqrt{s_{NN}}$.

The four-dimensional iso-energy density spacetime surface is constructed using the Cornelius hypersurface finder [23]. From this hypersurface, the particle distributions are generated according to the Cooper-Frye formula. Rescatterings and final decays of these particles are then computed in UrQMD. The end result is a distribution of particles which is directly comparable against the experimental data.

The dynamic change in the importance of the non-equilibrium transport and the hydrodynamic part of the evolution and having a proper equation of state applicable at high net baryon densities are the main advantages of this hybrid approach. As it is enough for the purposes of this study to reach a qualitative agreement with the experimental results, we neglect the viscosity effects during the hydrodynamical evolution. The high viscosity in the hadron gas phase is included, however.

Compared to the previous investigations of the elliptic flow using the same hybrid approach [24, 25], the new features in this study are the new implementation of the Cooper-Frye hypersurface finder and particlization, described above, and replacing the reaction plane (RP) analysis with the event plane (EP) method [26, 27] when computing v_2 and v_3 from the particle momentum distributions.

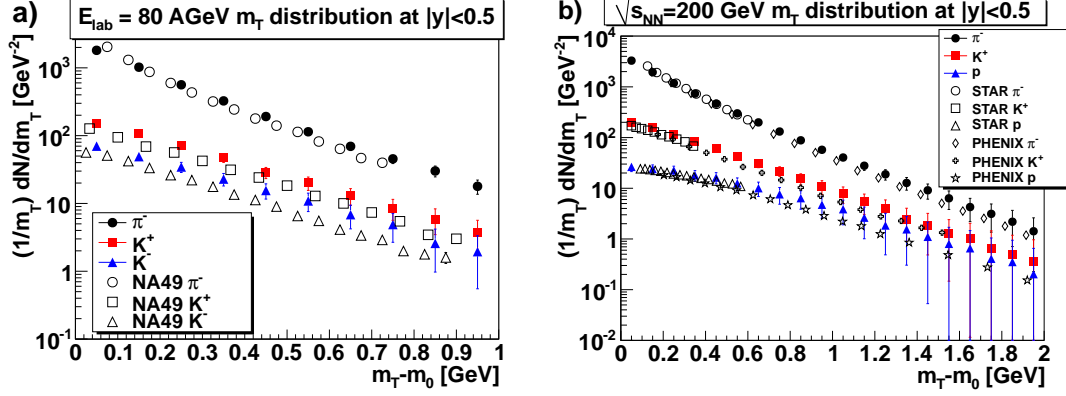


FIG. 1: (Color online) Transverse mass m_T -spectra at midrapidity $|y| < 0.5$. a) m_T -spectra for π^- , K^+ and K^- in Pb+Pb -collisions with impact parameter $b = 0 - 4$ fm, compared to the NA49 data [28] at beam energy $E_{\text{lab}} = 80$ AGeV. b) m_T -spectra for π^- , K^+ and p in $\sqrt{s_{NN}} = 200$ GeV Au+Au -collisions with impact parameter $b = 0 - 3.4$ fm, compared to the 0-5% centrality data from STAR [29] and PHENIX [30].

III. RESULTS

A. Particle spectra

Our first step is to check how well the current setup of the hybrid model reproduces experimental data for bulk observables. The m_T spectra at midrapidity $|y| < 0.5$ for π^- , K^+ and K^- in Pb+Pb -collisions with beam energy $E_{\text{lab}} = 80$ AGeV (corresponding to the collision energy $\sqrt{s_{NN}} \approx 12$ GeV) is illustrated in Figure 1a. A good agreement with the NA49 data [28] is found, although the pion slope is a little too flat and there is an excess of kaons produced. Similar results are found for π^- , K^+ and p in $\sqrt{s_{NN}} = 200$ GeV Au+Au -collisions, as shown in Figure 1b. For the purpose of the current investigation the agreement with the experimental data is sufficient; for future studies the particlization energy density value can be adjusted to achieve a better agreement with the measured spectra.

B. Elliptic flow

Figure 2 shows the hybrid model result for the integrated elliptic flow $v_2\{\text{EP}\}$ for charged particles with transverse momentum $0.2 \text{ GeV} < p_T < 2.0 \text{ GeV}$ produced in Au+Au -collisions in $|\eta| < 1.0$ pseudorapidity, compared with the STAR data for three centrality

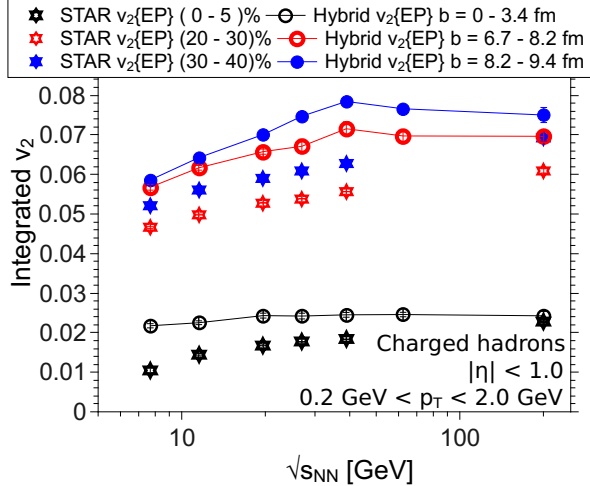


FIG. 2: (Color online) Integrated elliptic flow $v_2\{EP\}$ for charged hadrons with $0.2 < p_T < 2.0$ at midrapidity $|\eta| < 1.0$ in Au+Au -collisions, for collision energies $\sqrt{s_{NN}} = 7.7 - 200$ GeV and three different impact parameter ranges, compared with the STAR data [7, 33].

classes: (0-5)%, (20-30)% and (30-40)%. These centralities are respectively represented by the impact parameter intervals $b = 0 - 3.4$ fm, $b = 6.7 - 8.2$ fm and $b = 8.2 - 9.4$ fm in the model, where the choice of values is based on the optical Glauber model estimates [31, 32].

With the chosen parameters, the hybrid model systematically overshoots the experimental data. The examination of the $v_2(p_T)$ produced by the simulations (Figure 3) reveals that the overshoot is worse at higher p_T , while at the lower limit of the p_T -cut the produced flow agrees with the data. It remains as a question for a future study to see if both the particle spectra and the flow can be made to match the data with the same choice of parameters; likely the viscous corrections will prove to be necessary. However, for this investigation the most important thing is the qualitative agreement with the data – for midcentral collisions, the observed modest collision energy dependence is well reproduced by the model. In the most central collisions, the elliptic flow energy dependence is even weaker than in experiments, to the point of being almost constant.

In order to understand why the elliptic flow appears to change so little over such a large range of beam energies, we investigate in more detail the contributions from the different phases of the heavy ion collision event on this observable. Figure 4 demonstrates the magnitude of v_2 before the hydrodynamical evolution, right after particlization and finally after the hadronic rescatterings performed in the UrQMD (the end result). In the most central

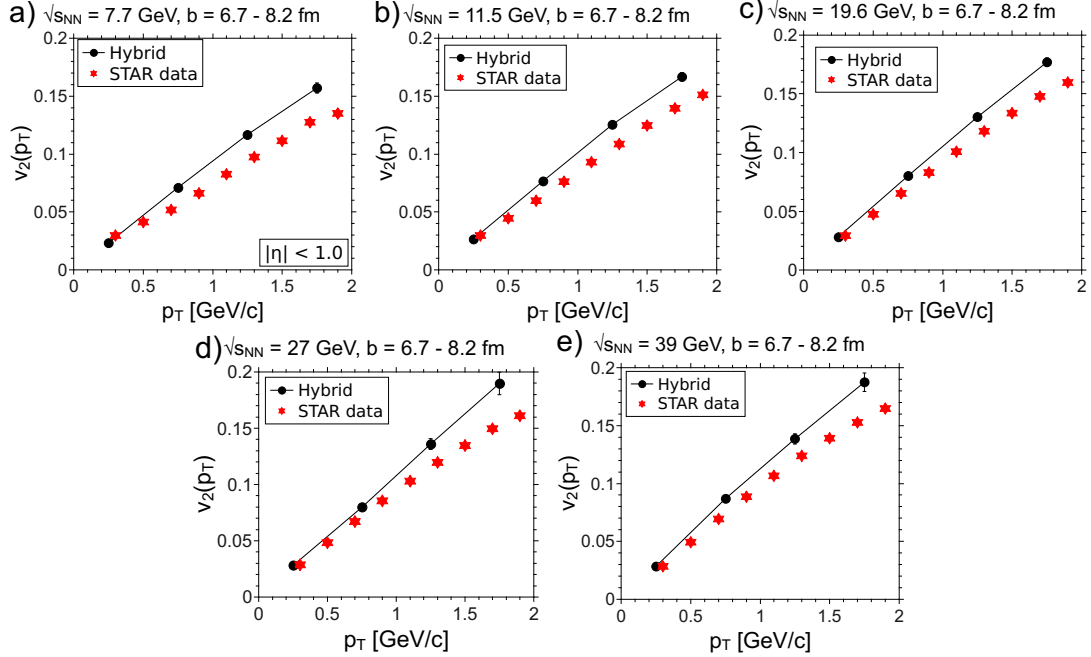


FIG. 3: (Color online) (a-e) Differential $v_2\{\text{EP}\}$ at midrapidity $|\eta| < 1.0$ for collision energies $\sqrt{s_{NN}} = 7.7 - 39$ GeV in impact parameter range $b = 6.7 - 8.2$ fm, compared with the STAR data in (20-30)% centrality [7].

collisions, where the overall elliptic flow is small compared to mid-central collisions, the effect of the hadronic rescatterings is negligible. In the impact parameter range $b = 8.2 - 9.4$ fm the contribution from the hadronic rescatterings is about 10%.

In both centralities, the hydrodynamic phase contributes very little to the elliptic flow at $\sqrt{s_{NN}} = 5 - 7.7$ GeV; v_2 at 5 GeV is in practice completely produced by the transport dynamics. However, already at $\sqrt{s_{NN}} = 11.5$ GeV the contribution from the hydrodynamics is significant in non-central collisions. It thus seems that the hydrodynamically produced v_2 *does* vanish at low collision energies, as was the naive expectation. The measured v_2 still remains nonzero, however, as the transport dynamics become more important at lower energies and are able to compensate for the reduction of hydrodynamically produced flow. Indeed, a recent study by Denicol *et al.* suggests that the hadron resonance gas with a large baryon number density can have more ideal fluid-like behavior compared to the same gas at zero baryon number density [14].

To make a connection with the earlier reaction plane analyses [24, 25], Figure 5 shows the integrated reaction plane v_2 for the present version of the hybrid, compared with the UrQMD

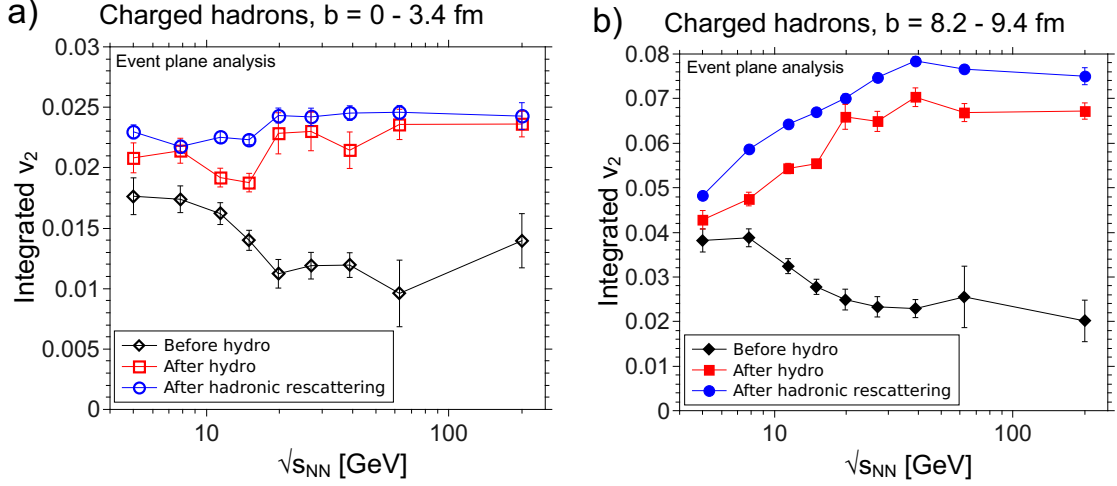


FIG. 4: (Color online) Magnitude of $v_2\{\text{EP}\}$ at the beginning of hydrodynamical evolution (diamonds), immediately after particlization (squares) and after the full simulation (circles, the same as in Fig. 2) at a) central collisions and b) midcentral collisions.

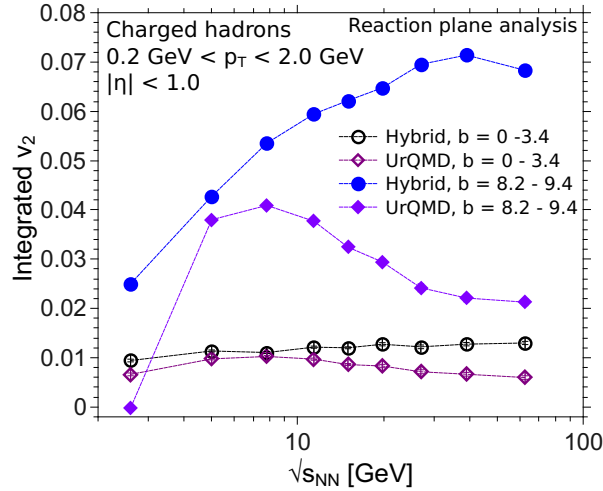


FIG. 5: (Color online) Comparison of $v_2\{\text{RP}\}$ produced in hybrid (circles) and in UrQMD without hydro (diamonds).

result without hydrodynamics. This comparison also demonstrates that for $\sqrt{s_{NN}} = 5$ GeV, the contribution from hydrodynamics is nearly negligible. At the even lower energy $E_{\text{lab}} = 2$ GeV the hybrid again produces more flow; however, the applicability of ideal hydrodynamics for the whole system at such a low energy begins to be questionable. At lower energies a dynamical switching between non-equilibrium transport and fluid dynamics is necessary which is beyond the current capabilities of the hybrid model.

C. Triangular flow

The triangular flow v_3 is a good observable for measuring the system sensitivity to the initial state fluctuations, as it is generated solely by event-by-event variations in the initial configuration of the colliding nucleons. Compared to the elliptic flow, triangular flow is considerably less sensitive to the overall collision geometry; it is, however, also harder to measure reliably due to having a smaller magnitude.

The $\sqrt{s_{NN}}$ -dependence of the integrated $v_3\{\text{EP}\}$ produced by the hybrid model for impact parameter ranges $b = 0 - 3.4$ fm and $b = 6.7 - 8.2$ fm is presented in Figure 6a. In the most central collisions, v_3 increases only slightly from below 0.01 to 0.015 with increasing collision energy, whereas in midcentrality there is a rapid rise from ≈ 0 at $\sqrt{s_{NN}} = 5$ GeV to the value of ≈ 0.02 for $\sqrt{s_{NN}} \geq 27$ GeV. The values at $\sqrt{s_{NN}} = 200$ GeV are in agreement with the experimental data [34]. The energy dependence of midcentral v_3 is very similar to what was seen for the hydrodynamically produced v_2 in Figure 4b, suggesting that in this case the transport part of the model is unable to compensate for the diminished hydro phase.

Like v_3 , the event plane elliptic flow $v_2\{\text{EP}\}$ is also affected by the initial state fluctuations, as the event plane angle (and thus the tilt of the v_2 -generating ellipsoid) varies event-by-event. The reaction plane v_2 , on the other hand, is insensitive to these variations. Based on [35–37], we (ignoring nonflow effects) define the contribution of fluctuations to v_2 as

$$\sigma_{v_2} = \sqrt{\frac{1}{2}(v_2\{\text{EP}\}^2 - v_2\{\text{RP}\}^2)}, \quad (2)$$

and compare the magnitudes of the two fluctuation-based observables in Figure 6b. We find σ_{v_2} remaining nearly constant with respect to the collision energy. Within the statistical uncertainties, $v_3\{\text{EP}\} = \sigma_{v_2}$ at $\sqrt{s_{NN}} \geq 27$ GeV. Thus the system is able to convert the initial state fluctuations to v_2 at all energies, but for v_3 the task becomes increasingly more difficult with lower $\sqrt{s_{NN}}$.

D. Flow dependence on initial geometry

Based on the above comparison of fluctuation-generated σ_{v_2} and v_3 , the relationship between the flow coefficients and the initial collision geometry warrants more investigation.

Figure 7 illustrates the collision energy and centrality dependencies of the event-averaged

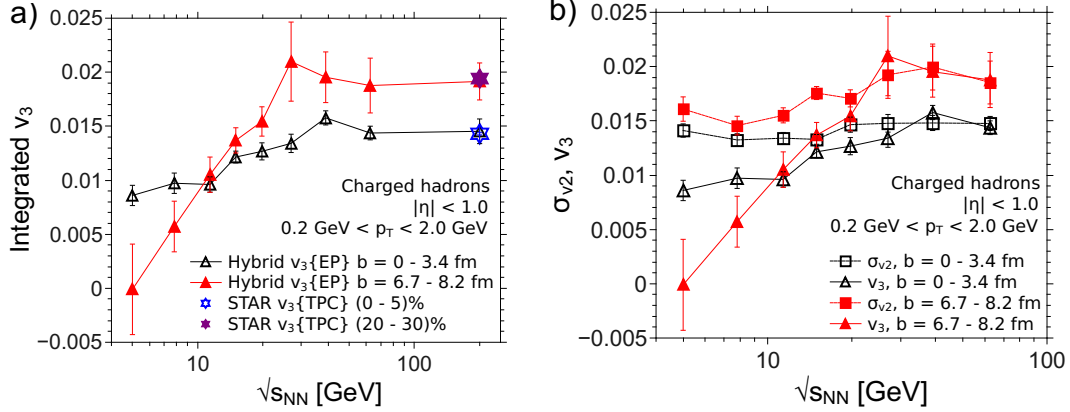


FIG. 6: (Color online) a) Integrated $v_3\{\text{EP}\}$ at midrapidity $|\eta| < 1.0$ in central collisions ($b = 0 - 3.4$ fm, open triangles) and midcentral collisions ($b = 6.7 - 8.2$ fm, solid triangles), compared with the STAR data [34] (stars). b) $v_3\{\text{EP}\}$ compared with initial state fluctuations' contribution to v_2 , $\sigma_{v_2} = \sqrt{\frac{1}{2}(v_2\{\text{EP}\}^2 - v_2\{\text{RP}\}^2)}$ (squares).

initial state spatial eccentricity $\langle \epsilon_2 \rangle$ and triangularity $\langle \epsilon_3 \rangle$. The eccentricity and triangularity in an event, calculated at the beginning of the hydrodynamical evolution t_{start} , are defined by [38]:

$$\epsilon_n = \frac{\sqrt{\langle r^n \cos(n\phi) \rangle^2 + \langle r^n \sin(n\phi) \rangle^2}}{\langle r^n \rangle}, \quad (3)$$

where (r, ϕ) are the polar coordinates of the participant particles in the event and $\langle \dots \rangle$ denotes the average over the particles.

In the most central collisions, the collision area is nearly circular; both the average eccentricity and triangularity are created purely by the fluctuations in the spatial orientation of colliding nucleons and are similar in magnitude. At mid-central collisions, the overlap region of the colliding nuclei is almond-shaped, making $\langle \epsilon_2 \rangle$ clearly larger than $\langle \epsilon_3 \rangle$. As neither the typical spatial distribution of binary collisions, nor the inelastic nucleon-nucleon cross section σ_{NN} change significantly within the examined energy range, one expects only a weak dependence on the collision energy.

The hydro starting time t_{start} , however, is sensitive to the beam energy, dropping from 5.19 fm at $\sqrt{s_{NN}} = 5$ GeV to 1.23 fm at $\sqrt{s_{NN}} = 19.6$ GeV [15]. Thus the main reason for the systematic decrease of $\langle \epsilon_2 \rangle$ and $\langle \epsilon_3 \rangle$ seen at low energies in Fig. 7 is the longer transport evolution before the start of the hydrodynamical phase. During this evolution finite v_2 and v_3 values are built up that quench the initial eccentricity and triangularity.

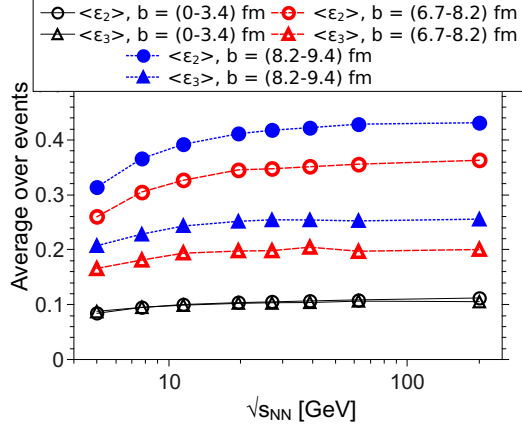


FIG. 7: (Color online) Average eccentricity $\langle \epsilon_2 \rangle$ (circles) and triangularity $\langle \epsilon_3 \rangle$ (triangles) as a function of collision energy $\sqrt{s_{NN}}$, for impact parameter ranges $b = 0 - 3.4$ fm (solid lines), $6.7 - 8.2$ fm (dashed lines) and $8.2 - 9.4$ fm (dotted lines).

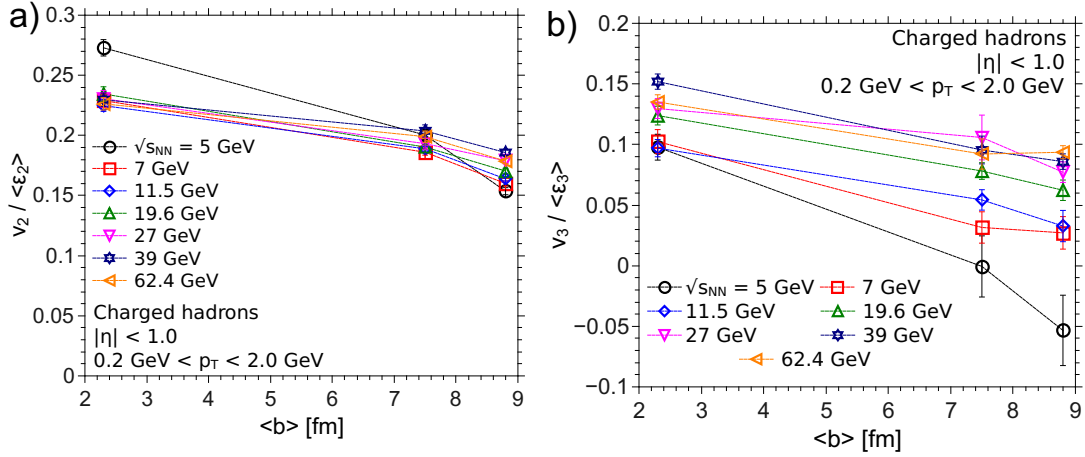


FIG. 8: (Color online) Energy evolution of a) v_2 {EP} scaled with average eccentricity $\langle \epsilon_2 \rangle$, and b) v_3 {EP} scaled with average triangularity $\langle \epsilon_3 \rangle$, as a function of average impact parameter $\langle b \rangle$.

In order to examine the system response to initial geometry, we scale v_2 and v_3 with $\langle \epsilon_2 \rangle$ and $\langle \epsilon_3 \rangle$, respectively. The result for the three centrality classes, represented by their average impact parameters $\langle b \rangle$, is shown in Figure 8. Aside from the anomalous most central point at $\sqrt{s_{NN}} = 5$ GeV, the relation of the elliptic flow to the initial eccentricity changes relatively little for the whole collision energy range, in comparison to the v_3 response to the triangularity of the initial state which shows a clear increase as one moves toward higher energies. This supports the idea that the hadron gas dynamics are sufficient for producing

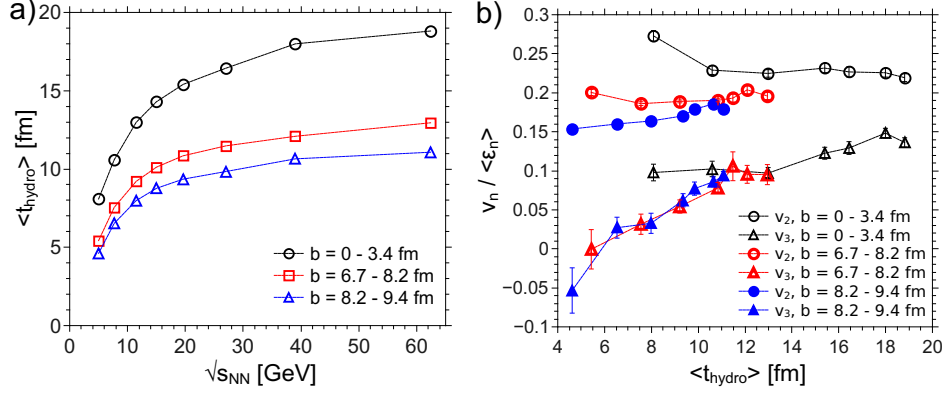


FIG. 9: (Color online) a) Average total duration $\langle t_{\text{hydro}} \rangle$ of the hydrodynamical phase in the simulation as a function of collision energy $\sqrt{s_{NN}}$. b) Scaled flow coefficients $v_2/\langle \epsilon_2 \rangle$ and $v_3/\langle \epsilon_3 \rangle$ with respect to the average total hydro duration for impact parameter ranges $b = 0 - 3.4$ fm, $6.7 - 8.2$ fm and $8.2 - 9.4$ fm.

the v_2 response to the collision geometry at low collision energies, but a less viscous fluid would be needed for producing the comparatively weaker v_3 response to triangularity at the same $\sqrt{s_{NN}}$.

To study the dependence of the flow coefficients on the existence of a hydrodynamic evolution in more detail, we plot, in Figure 9b, the scaled v_2 and v_3 with respect to the event-averaged total duration of hydrodynamical phase in the simulation $\langle t_{\text{hydro}} \rangle$, measured in the computational frame (Fig. 9a). It should be noted that this quantity represents the absolute upper limit of hydrodynamical phase in the simulation; as the particlization surface is not isochronous but iso-energy density, most of the system has been decoupled from the hydro long before t_{hydro} . For an example of the actual spacetime dependence of the particlization in the hybrid model, see Ref. [23].

It is seen in Fig. 9b that, with the exception of the most central collisions at $\sqrt{s_{NN}} = 5$ GeV, the scaled v_3 points form an uniform, monotonically increasing function of $\langle t_{\text{hydro}} \rangle$. For v_2 , the different centralities do not have such uniform behavior because of the additional elliptic flow produced by the transport part at low energies. In other words, the final triangular flow is purely a product of hydrodynamics at all beam energies, while the final elliptic flow at low $\sqrt{s_{NN}}$ is not.

IV. SUMMARY

In this article, we have investigated the collision energy dependence of the flow coefficients v_2 and v_3 in a hybrid transport + hydrodynamics approach. In such a framework, it is seen that the hadron / string pre-equilibrium dynamics can compensate for the diminished hydrodynamical evolution for v_2 production at lower collision energies. Because of this, v_2 changes relatively little as a function of beam energy. This remains true for v_2 scaled with the average eccentricity $\langle\epsilon_2\rangle$, as the initial eccentricity also changes very modestly for the most of the examined collision energy range, decreasing more steeply only below $\sqrt{s_{NN}} \lesssim 10$ GeV, where the pre-equilibrium phase lasts for several fm.

For the triangular flow v_3 , generated purely by the spatial configuration fluctuations of the colliding nucleons in the initial state, it is found that the system response to initial triangularity begins decreasing below $\sqrt{s_{NN}} = 27$ GeV, reaching ≈ 0 for midcentral collisions at $\sqrt{s_{NN}} = 5$ GeV. In addition, the scaled v_3 points over several collision energies and centrality classes form an uniform function of the hydro duration $\langle t_{\text{hydro}} \rangle$, whereas for the elliptic flow the relation is distorted by the transport dynamics. Thus, compared to v_2 , the triangular flow provides a clearer signal for the formation of (near-)ideal fluid in heavy ion collisions.

For the future studies, the issues with kaon production and $v_2(p_T)$ overestimating the data at higher p_T will necessitate a slight re-tuning of the model parameters and possibly the addition of viscous corrections to the hydrodynamical phase for the optimal agreement with the experimental data. Also, while the values for the triangular flow v_3 at high collision energies (and also at the lower limit $\sqrt{s_{NN}} = 7.7$ GeV) quantitatively agree with the experimental results, there is a qualitative disagreement with the preliminary STAR data, where no beam energy dependence is seen within 0-5%, 5-10% or 10-20% centrality at $\sqrt{s_{NN}} = 7.7 - 27$ GeV [8].

As the hadron resonance gas has proven to be too viscous for producing v_3 from initial state fluctuations in this investigation, the current discrepancy between the simulation results and the preliminary experimental data implies that larger quantities of low-viscous state of matter is manifested at lower collision energies than expected in this study. On the other hand, the inconsistent behavior of flow observables at $\sqrt{s_{NN}} = 5$ GeV compared to the higher energy points suggest that the lower energy limit of applicability may have been

reached for the ideal hydrodynamics approach. More detailed studies, both theoretical and experimental, are thus needed for v_3 at $\sqrt{s_{NN}} \leq 10$ GeV energies.

V. ACKNOWLEDGEMENTS

We thank H. Holopainen, Iu. A. Karpenko and P. Huovinen for useful discussions. The authors acknowledge funding of the Helmholtz Young Investigator Group VH-NG-822. This work was supported by the Helmholtz International Center for the Facility for Antiproton and Ion Research (HIC for FAIR) within the framework of the Landes-Offensive zur Entwicklung Wissenschaftlich-ökonomischer Exzellenz (LOEWE) program launched by the State of Hesse. Computational resources have been provided by the Center for Scientific Computing (CSC) at the Goethe-University of Frankfurt.

-
- [1] Z. Fodor and S. D. Katz, JHEP **0404**, 050 (2004).
 - [2] S. Ejiri, Phys. Rev. D **78**, 074507 (2008).
 - [3] R. V. Gavai and S. Gupta, Phys. Rev. D **78**, 114503 (2008).
 - [4] Y. Aoki, G. Endrodi, Z. Fodor, S. D. Katz and K. K. Szabo, Nature **443**, 675 (2006).
 - [5] G. Endrodi, Z. Fodor, S. D. Katz and K. K. Szabo, JHEP **1104**, 001 (2011).
 - [6] G. Odyniec, J. Phys. Conf. Ser. **455**, 012037 (2013).
 - [7] L. Adamczyk *et al.* [STAR Collaboration], Phys. Rev. C **86**, 054908 (2012).
 - [8] Y. Pandit [STAR Collaboration], talk at Quark Matter 2012.
 - [9] V. P. Konchakovski, E. L. Bratkovskaya, W. Cassing, V. D. Toneev, S. A. Voloshin and V. Voronyuk, Phys. Rev. C **85**, 044922 (2012).
 - [10] C. Shen and U. Heinz, Phys. Rev. C **85**, 054902 (2012) [Erratum-ibid. C **86**, 049903 (2012)].
 - [11] D. Solanki, P. Sorensen, S. Basu, R. Raniwala and T. K. Nayak, Phys. Lett. B **720**, 352 (2013).
 - [12] S. Plumari, V. Greco and L. P. Csernai, arXiv:1304.6566 [nucl-th].
 - [13] R. A. Lacey, A. Taranenko, J. Jia, D. Reynolds, N. N. Ajitanand, J. M. Alexander, Y. Gu and A. Mwai, arXiv:1305.3341 [nucl-ex].
 - [14] G. S. Denicol, C. Gale, S. Jeon and J. Noronha, arXiv:1308.1923 [nucl-th].

- [15] H. Petersen, J. Steinheimer, G. Burau, M. Bleicher and H. Stöcker, Phys. Rev. C **78**, 044901 (2008).
- [16] S. A. Bass, M. Belkacem, M. Bleicher, M. Brandstetter, L. Bravina, C. Ernst, L. Gerland and M. Hofmann *et al.*, Prog. Part. Nucl. Phys. **41**, 255 (1998).
- [17] M. Bleicher, E. Zabrodin, C. Spieles, S. A. Bass, C. Ernst, S. Soff, L. Bravina and M. Belkacem *et al.*, J. Phys. G **25**, 1859 (1999).
- [18] H. Petersen, C. Coleman-Smith, S. A. Bass and R. Wolpert, J. Phys. G **38**, 045102 (2011).
- [19] D. H. Rischke, S. Bernard and J. A. Maruhn, Nucl. Phys. A **595**, 346 (1995).
- [20] D. H. Rischke, Y. Pursun and J. A. Maruhn, Nucl. Phys. A **595**, 383 (1995) [Erratum-ibid. A **596**, 717 (1996)].
- [21] J. Steinheimer, S. Schramm and H. Stöcker, Phys. Rev. C **84**, 045208 (2011).
- [22] J. Steinheimer, V. Dexheimer, M. Bleicher, H. Petersen, S. Schramm and H. Stöcker, Phys. Rev. C **81**, 044913 (2010).
- [23] P. Huovinen and H. Petersen, Eur. Phys. J. A **48**, 171 (2012).
- [24] H. Petersen and M. Bleicher, Phys. Rev. C **79**, 054904 (2009).
- [25] H. Petersen and M. Bleicher, Phys. Rev. C **81**, 044906 (2010).
- [26] A. M. Poskanzer and S. A. Voloshin, Phys. Rev. C **58**, 1671 (1998).
- [27] J. -Y. Ollitrault, nucl-ex/9711003.
- [28] S. V. Afanasiev *et al.* [NA49 Collaboration], Phys. Rev. C **66**, 054902 (2002).
- [29] J. Adams *et al.* [STAR Collaboration], Phys. Rev. Lett. **92**, 112301 (2004).
- [30] S. S. Adler *et al.* [PHENIX Collaboration], Phys. Rev. C **69**, 034910 (2004).
- [31] K. J. Eskola, K. Kajantie and J. Lindfors, Nucl. Phys. B **323**, 37 (1989).
- [32] D. Miskowiec, <http://web-docs.gsi.de/~misko/overlap/>
- [33] J. Adams *et al.* [STAR Collaboration], Phys. Rev. C **72**, 014904 (2005).
- [34] L. Adamczyk *et al.* [STAR Collaboration], Phys. Rev. C **88**, 014904 (2013).
- [35] R. S. Bhalerao and J. -Y. Ollitrault, Phys. Lett. B **641**, 260 (2006).
- [36] S. A. Voloshin, A. M. Poskanzer, A. Tang and G. Wang, Phys. Lett. B **659**, 537 (2008).
- [37] J. -Y. Ollitrault, A. M. Poskanzer and S. A. Voloshin, Phys. Rev. C **80**, 014904 (2009).
- [38] H. Petersen, G. -Y. Qin, S. A. Bass and B. Muller, Phys. Rev. C **82**, 041901 (2010).